energies

MDPI

Article

Enhancing MPPT Performance in Partially Shaded PV Systems under Sensor Malfunctioning with Fuzzy Control

Moazzam Ali Rabbani [1], Muhammad Bilal Qureshi [1,*], Salman A. Al Qahtani [2], Muhammad Mohsin Khan [3] and Pranavkumar Pathak [4]

[1] Department of Electrical and Computer Engineering, COMSATS University Islamabad, Abbottabad Campus, Abbottabad 22060, Pakistan; moazzamrabbani@gmail.com
[2] Department of Computer Engineering, College of Computer and Information Sciences, King Saud University, Riyadh 11543, Saudi Arabia; salmanq@ksu.edu.sa
[3] Department of IT & CS, FECID, PAF-IAST, Haripur 22620, Pakistan; mohsin.khan@spcai.paf-iast.edu.pk
[4] School of Continuing Studies, McGill University, Montreal, QC H3A 0G4, Canada; pranavkumar.pathak@mail.mcgill.ca
* Correspondence: bilalqureshi@cuiatd.edu.pk

Abstract: The shift towards sustainable energy sources is gaining momentum due to their environmental cleanliness, abundant availability, and eco-friendly characteristics. Solar energy, specifically harnessed through photovoltaic (PV) systems, emerges as a clean, abundant, and environmentally friendly alternative. However, the efficacy of PV systems is subjective depending on two critical factors: irradiance and temperature. To optimize power output, maximum power point tracking (MPPT) strategies are essential, allowing operation at the system's optimal point. In the presence of partial shading, the power–voltage curve exhibits multiple peaks, yet only one global maximum power point (GMPP) can be identified. Existing algorithms for GMPP tracking often encounter challenges, including overshooting during transient periods and chattering during steady states. This study proposes the utilization of fuzzy sliding mode controllers (FSMC) and fuzzy proportional-integral (FPI) control to enhance global MPPT reference tracking under partial shading conditions. Additionally, the system's performance is evaluated considering potential sensor malfunctions. The proposed techniques ensure precise tracking of the reference voltage and maximum power in partial shading scenarios, facilitating rapid convergence, improved system stability during transitions, and reduced chattering during steady states. The usefulness of the proposed scheme is confirmed through the use of performance indices. FSMC has the lowest integral absolute error (IAE) of 946.94, followed closely by FPI (947.21), in comparison to the sliding mode controller (SMC) (1241.6) and perturb and observe (P&O) (2433.1). Similarly, in integral time absolute error (ITAE), FSMC (56.84) and FPI (57.06) excel over SMC (91.03) and P&O (635.50).

Keywords: fuzzy PI; fuzzy sliding mode controller; maximum power point tracking; partial shading; global maximum power point tracking

Citation: Rabbani, M.A.; Qureshi, M.B.; Al Qahtani, S.A.; Khan, M.M.; Pathak, P. Enhancing MPPT Performance in Partially Shaded PV Systems under Sensor Malfunctioning with Fuzzy Control. *Energies* **2023**, *16*, 4665. https://doi.org/10.3390/en16124665

Academic Editor: Carlo Renno

Received: 28 April 2023
Revised: 7 June 2023
Accepted: 9 June 2023
Published: 12 June 2023

1. Introduction

In the past few years, as the demand for energy has escalated, the worldwide use of fossil fuel resources has peaked, and locating fresh reserves has become difficult. The threat of fossil fuel depletion and the associated impacts of global warming caused by hazardous gas emissions have compelled the consideration of alternative energy sources [1,2]. Conventional and non-conventional energy resources are available for energy generation. Conventional energy resources include coal, oil, thermal, and nuclear power. Non-conventional energy resources encompass solar, geothermal, biomass, wind, and tidal energy. These sources are also known as renewable energy sources because they generate energy without negatively affecting the environment [3–5].

Amongst the aforementioned sustainable energy sources [6], photovoltaic energy emerges as a crucial energy resource. Energy forecasts indicate that the capacity of photovoltaic (PV) systems will surpass wind energy production [7].

The efficiency of solar panel output is influenced by a variety of parameters, among which the most important is maximum power point tracking (MPPT). Partial shading occurs when a portion of a PV system's array is obscured by shadows cast by surrounding objects, such as trees, buildings, and passing clouds [8]. Solar irradiance and temperature are the two main factors that have an external impact on the output of a PV array [9]. These external factors cause the MPP of PV panels to shift. When a PV system is partially shaded, the power–voltage characteristic curve forms various peaks. Within these peaks, there exists only one global maximum power point (GMPP), whereas the remaining ones are known as local MPPs [10], as shown in Figure 1.

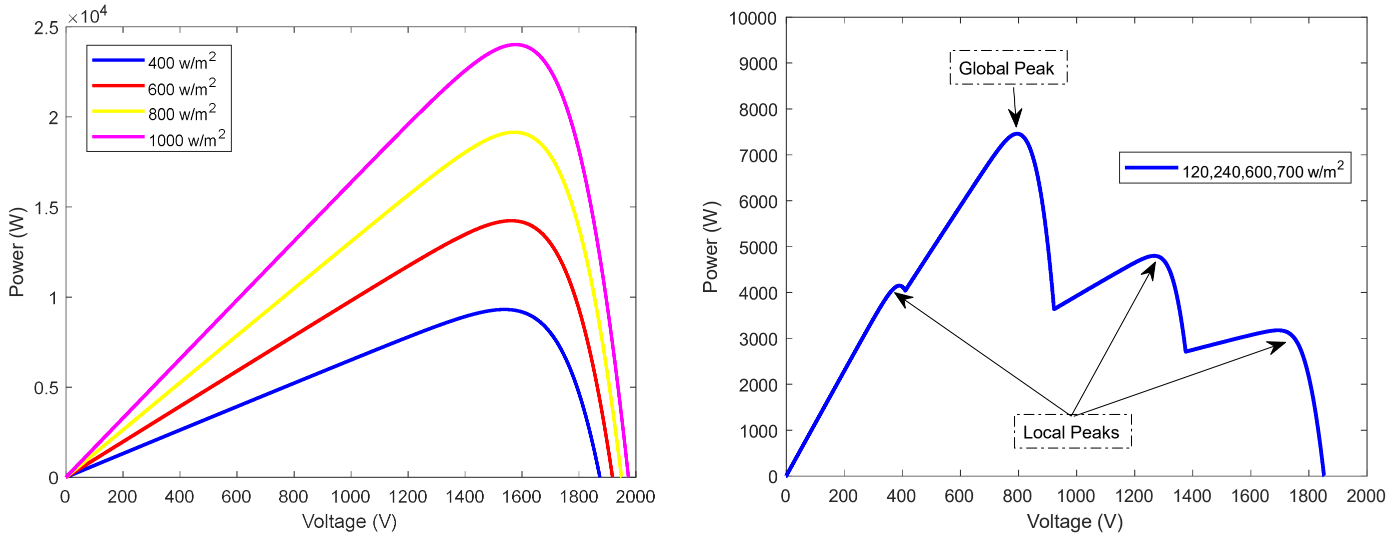

(**a**) (**b**)

Figure 1. (**a**) Under uniform isolation, characteristics of P–V curve for PV array; (**b**) under partial shading conditions, characteristics of P–V curve for PV array.

In this situation, it is possible that the PV array is operating at its local maximum power point (LMPP). The existence of multiple maximum power points reduces the effectiveness of the tracking algorithm. In the case of the existence of multiple peaks, it is challenging for an algorithm to determine the best global maximum power point (GMPP) among the ones available. Many strategies and algorithms have been used in order to maximize the solar panel's output, and they have had some success in achieving their goal.

An adaptive particle swarm optimization (APSO) was proposed by Roy Chowdhury et al. in [11] to track the global maximum power point (GMPP) in varied weather situations. Due to the complexity of the mathematical calculations and approximations involved, it takes longer to monitor the accuracy and steady-state inaccuracy, making it difficult to implement. In [12], Safari used the variable step size incremental conductance approach to analyze the GMPP. It automatically adjusts the step size to strike a reasonable balance between monitoring dynamics and energy loss reduction. When the PV array includes many local maximum power points, the linear function might not be able to locate the point nearest to the GMPP. The developers of [13,14] used population-based methods, such as ant colony optimization (ACO), particle swarm optimization (PSO), and genetic algorithms (GAs), to obtain the maximum possible power. However, constructing these algorithms is exceedingly difficult due to their intricate nature, slow rate of convergence, and the necessity for extensive parameter adjustment, which renders them vulnerable to disturbances. Furthermore, all of these population-based algorithms demonstrate inefficiency in control problems, primarily due to their inadequate capacity to handle uncertainty and nonlinear systems proficiently, as well as their limited adaptability to dynamic environmental conditions. Ouahib Guenounou et al., the authors of [15], suggested MPPT using the adaptive fuzzy logic controller (AFLC), which is divided into two rules: one regulates the converter duty cycle, and the other regulates the controller gain. However, neither of these rules can eliminate chattering from the MPP due to the inherent characteristics and limitations of AFLC.

Naghmash et al. proposed a backstepping-based nonlinear controller; however, this controller still fails to provide the necessary output without chattering, steady-state inaccuracy, and oscillation, thereby compromising its effectiveness [16]. Syafaruddin et al. used a hybrid artificial neural network and fuzzy logic controller to track the GMPP [17]. These soft computing algorithms performed well in terms of tracking the maximum power. However, the complexity of these algorithms grows in proportion to the amount of data supplied into them. Furthermore, the massive amount of data that are provided increases the storage strain [18]. To maximize power in conditions of varying load and partial shading, the authors of [19] proposed the sliding mode control (SMC) technique, which is based on a simple sliding surface. The variable switching frequency of the suggested method makes filter design challenging and causes the chattering phenomenon [20]. To lessen the steady state inaccuracy, the authors of [21] added an integral term to the sliding surface. However, this pulse with a modulator-based controller exhibits an overshot problem.

In [22], model predictive control (MPC) was developed to improve the extraction of maximum power from PV arrays. When compared to traditional control schemes, the MPC technique offers a quick, dynamic reaction with a relatively high stability margin, which makes it more suitable for MPPT of PV systems working in rapidly changing atmospheric circumstances [23]. However, this technique also possesses a number of open instability issues, especially when the operating point is not close to the tracked reference [24].

This study of the literature leads to the conclusion that several GMPP tracking approaches have been developed with various characteristics, such as complexity, sensing material, convergence time, performance, cost, and compatibility, to detect the GMPP under partial shading situations. Although each approach has its own advantages and disadvantages, all traditional techniques share the common issues of chattering and slow convergence.

The main contributions of the proposed work to address the chattering and convergence issues are as follow:

1. Fuzzy PI (FPI) and fuzzy sliding mode controller (FSMC) for MPPT: This study introduces the utilization of FPI and FSMC as controllers for effectively tracking the global maximum power from a partially shaded PV system. These controllers offer a reliable and efficient solution for MPPT under partial shading conditions (PSCs), ensuring quick and finite-time convergence.
2. Neural network-based reference voltage generation: A neural network is employed to generate the reference voltage for maximum power point tracking. The system's resilience and chattering minimization capabilities are evaluated by introducing uncertainties into the system and faults in the sensors. The proposed controllers demonstrate their effectiveness under challenging operating conditions, providing accurate tracking of the reference voltage and maximum power, particularly in the presence of partial shading.
3. Performance evaluation and comparison: The performance of the proposed controllers is assessed by calculating and comparing various performance indices. Simulation results are analyzed, and a comparison is made with conventional controllers, such as perturb and observe (P&O) and the standard sliding mode controller. The effectiveness of the proposed technique in terms of superior performance is characterized by reduced chattering, improved transient responsiveness, enhanced tracking precision, and faster convergence.

2. System Modelling

The KYOCERA KC200GT module is used for the PV system. Four PV arrays are connected in the series for the proposed PV system. Each array consists of two parallel (Np) and fifteen series (Ns) modules. Each PV array generates 6 KW at nominal conditions (25 °C at 1000 W/m^2). The total output of the PV arrays is 24 KW. Mathematical modelling of the PV array and its parameters is given in Appendix A.

2.1. Mathematical Modelling of the Buck–Boost Converter

A given DC voltage can be converted to both step-up and step-down voltages by the buck–boost converter non-inverting configuration [25]. The utilized converter circuit consists of two switches (first, switch S_1, and second, S_2) and two capacitors (first, capacitor C_1, and second, C_2), as shown in Figure 2. Two diodes (D_1 and D_2) are also included in the design. Under the assumption of continuous conduction mode (CCM), all operations are supposed to be carried out. It operates in two switching modes. S_1 and S_2 are both closed (ON) in mode 1, and S_1 and S_2 are both open (OFF) in mode 2.

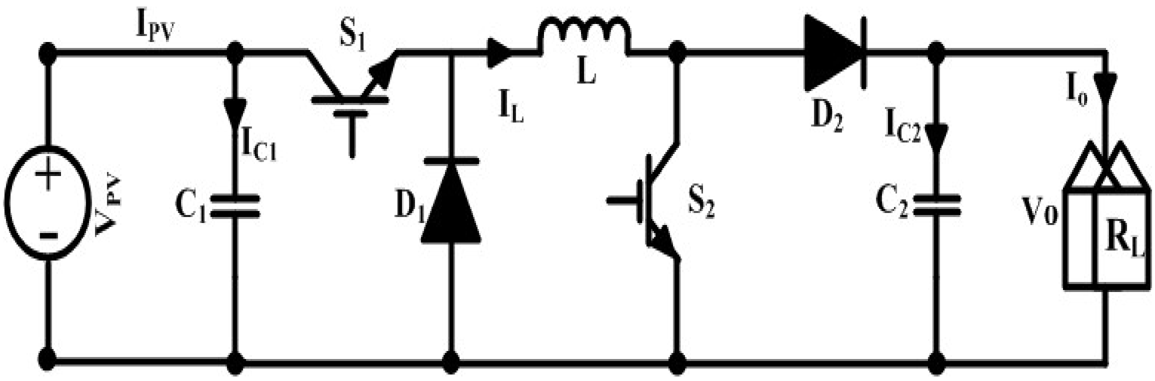

Figure 2. Buck–boost converter non-inverting circuit configuration.

In the first mode, all the switches, which are S_1 and S_2, are turned on, while both the diodes, which are D_1 and D_2, are turned off (reverse biased). According to the law of energy conservation,

$$\begin{cases} I_{C_1} = I_{pv} - I_L \\ V_L = V_{C_1} \\ I_{C_2} = -\frac{V_{C_2}}{R} \end{cases} \tag{1}$$

where I_{C_1}, I_{C_2}, I_{pv}, and I_L are the current of capacitor C_1, the current of capacitor C_2, the current of the PV panel, and the current of inductor L, respectively. V_L, V_{C_1}, and V_{C_2} are the voltage across the inductors, the voltage across the C_1, and the voltage across the C_2, respectively.

In mode 2, both diodes (D_1 and D_2) are on (forward bias) and both switches (S_1 and S_2) are off, and we obtain,

$$\begin{cases} I_{C_1} = I_{pv} \\ V_L = V_{C_2} \\ I_{C_2} = I_L - \frac{V_{C_2}}{R} \end{cases} \tag{2}$$

where R is the load resistance.

The above equations can be expressed as follows by utilizing the capacitor charge balance and inductor voltage balance principles,

$$\begin{cases} \frac{dV_{C_1}}{dt} = \frac{I_{pv}}{C_1} - \frac{I_L}{C_1}\mu \\ \frac{dI_L}{dt} = \frac{V_{C_1}}{L}\mu - \frac{V_{C_2}}{L}(1-\mu) \\ \frac{dV_{C_2}}{dt} = \frac{I_L}{C_2}(1-\mu) - \frac{V_{C_2}}{RC_2} \end{cases} \tag{3}$$

where C_1, C_2, and L are the capacitance of the first capacitor, the capacitance of the second capacitor, and the inductance of the inductor, respectively.

Using a single switching, we assume the following values for averaging the model,

$$\begin{cases} x_1 = \langle V_{C_1} \rangle \\ x_2 = \langle I_L \rangle \\ x_3 = \langle V_{C_2} \rangle \\ \mu = \langle u \rangle \end{cases} \tag{4}$$

To track the global peaks for maximum power, the non-inverting buck–boost converter state space average model is used by substituting $V_{C_2} = V_o$ and $C_1 = C_i$.

The vector-matrix representation of the mode 1 state space equation is as follows,

$$\begin{bmatrix} \frac{d}{dt} V_{pv} \\ \frac{d}{dt} I_L \\ \frac{d}{dt} V_o \end{bmatrix} = \begin{bmatrix} 0 & -\frac{1}{C_i} & 0 \\ \frac{1}{L} & 0 & 0 \\ 0 & 0 & 0 \end{bmatrix} \begin{bmatrix} V_{pv} \\ I_L \\ V_O \end{bmatrix} + \begin{bmatrix} \frac{I_{pv}}{C_i} \\ 0 \\ 0 \end{bmatrix} \tag{5}$$

The vector-matrix representation of the mode 2 state space equation is as follows,

$$\begin{bmatrix} \frac{d}{dt} V_{pv} \\ \frac{d}{dt} I_L \\ \frac{d}{dt} V_o \end{bmatrix} = \begin{bmatrix} 0 & -\frac{1}{C_i} & 0 \\ \frac{1}{L} & 0 & -\frac{1}{L} \\ 0 & \frac{1}{C_o} & 0 \end{bmatrix} \begin{bmatrix} V_{pv} \\ I_L \\ V_O \end{bmatrix} + \begin{bmatrix} \frac{I_{pv}}{C_i} \\ 0 \\ 0 \end{bmatrix} \tag{6}$$

The average converter model for both modes can be obtained by applying the principles of vector-matrix volt-second balance and capacitor charging balance equations to obtain the following form,

$$\begin{bmatrix} \frac{d}{dt} V_{pv} \\ \frac{d}{dt} I_L \\ \frac{d}{dt} V_o \end{bmatrix} = \begin{bmatrix} 0 & -\frac{u}{C_i} & 0 \\ \frac{u}{L} & 0 & \left(\frac{u}{L} - \frac{1}{L}\right) \\ 0 & \left(\frac{1}{C_o} - \frac{u}{C_o}\right) & -\frac{1}{R_L C_o} \end{bmatrix} \begin{bmatrix} V_{pv} \\ I_L \\ V_O \end{bmatrix} + \begin{bmatrix} \frac{I_{pv}}{C_i} \\ 0 \\ 0 \end{bmatrix} \tag{7}$$

The average values of V_{pv}, I_L, I_L, and u are represented by x_1, x_2, x_3, and u, respectively. The states are written in equation form as follows under this assumption,

$$\begin{bmatrix} \dot{x_1} \\ \dot{x_2} \\ \dot{x_3} \end{bmatrix} = \begin{bmatrix} 0 & -\frac{u}{C_i} & 0 \\ \frac{u}{L} & 0 & \left(\frac{u}{L} - \frac{1}{L}\right) \\ 0 & \left(\frac{1}{C_o} - \frac{u}{C_o}\right) & -\frac{1}{R_L C_o} \end{bmatrix} \begin{bmatrix} x_1 \\ x_2 \\ x_3 \end{bmatrix} + \begin{bmatrix} \frac{I_{pv}}{C_i} \\ 0 \\ 0 \end{bmatrix} \tag{8}$$

The following is the representation matrix in equation form,

$$\begin{cases} \dot{x_1} = \frac{I_{pv}}{C_i} - \frac{x_2}{C_i} u \\ \dot{x_2} = \frac{x_1}{L} u - \frac{x_3}{L} (1 - u) \\ \dot{x_3} = \frac{x_2}{L} (1 - u) - \frac{x_3}{R C_2} \end{cases} \tag{9}$$

2.2. *Reference Voltage Generation*

When environmental conditions undergo abrupt changes, the power–voltage (P–V) characteristic curve also undergoes changes. Sudden variations in climatic conditions result in alterations to the shading pattern of the PV system and the GMPP. To determine the reference voltage generation of PV arrays under partial shading conditions, we implemented four distinct shading patterns (G1, G2, G3, and G4) and applied a temperature (T) to the PV system. From the power–voltage curve, we identified the global maximum power point (GMPP) and the corresponding voltage. We manually generated and tested seven hundred different patterns at a temperature of 298.15 K (25 °C) and recorded the voltage values at

GMPP. The GMPP values obtained using multiple shading patterns at 298.15 K are listed in Table 1.

Table 1. Shading patterns for test scenarios.

Patterns	G1	G2	G3	G4	T (Kelvin)
SP1	600	600	1000	1000	298.15
SP2	200	400	600	1000	298.15
SP3	120	240	600	700	298.15
SP4	200	400	600	1000	298.15
SP5	600	600	1000	1000	298.15
SP6	1000	1000	1000	1000	298.15

The reason for manually generating these irradiance patterns and the temperature is because in the case of partial shading, the available real profile typically provides only one set of irradiance and temperature values with respect to time. However, to effectively demonstrate the performance of the proposed controller in handling partial shading scenarios, it is necessary to generate additional irradiances. This is because real profiles often lack the diversity of shading conditions that can occur in practical situations, such as those caused by cloud cover, building shade, tree shade, or passing airplanes. By manually generating additional irradiances, we can simulate different levels of shading, ranging from full sunlight to varying degrees of partial shading. This allows us to thoroughly evaluate and validate the proposed controller's capability to optimize the power output under different shading conditions. For predicting the reference voltage, we utilized the supervised learning characteristics of ANN.

This ANN model consists of five inputs, forty hidden neurons, and one output layer. We have given four irradiance and one temperature as the input and voltage at the GMPP as output to train the ANN for reference generation. To train the ANN, a Bayesian Regularization algorithm is used in MATLAB due to its fast and accurate training. In comparison to other algorithms, the least number of neurons is enough to train the ANN despite the fact of noisy data and inadequate information provided by the input to the neural network. More than seven hundred samples are used to train the ANN. It generates the reference voltage with the least mean square error (MSE), which is 4.0676×10^{-9}.

3. Proposed Controllers Design

3.1. Fuzzy PI Controller

3.1.1. Fuzzy Logic Controller (FLC)

It is hard to grasp the real-world/fuzzy issues. Fuzzy logic controller (FLC) has the benefit of not just relying on mathematical models but instead including human logical reasoning. Its ability to handle non-linearity and uncertainty is another benefit. When current models are unclear, complicated, or unreliable, FLC is better equipped to handle these situations. Fuzzification, rule base, interference engine, and defuzzification are the four stages of FLC design. Figure 3 depicts the fuzzy logic controller.

- The IF–THEN rules of the fuzzy system containing the condition and a conclusion are resolved in the rule base.
- A rule base is established for the output depending on the values of the inputs.
- An expert's choice in understanding and implementing the rules of the game is the focus of fuzzy inference. It is the process through which regulations are assessed and then discarded.
- To obtain real-time data out of the inference engine, we use an output mapping interface called a de-fuzzifier.

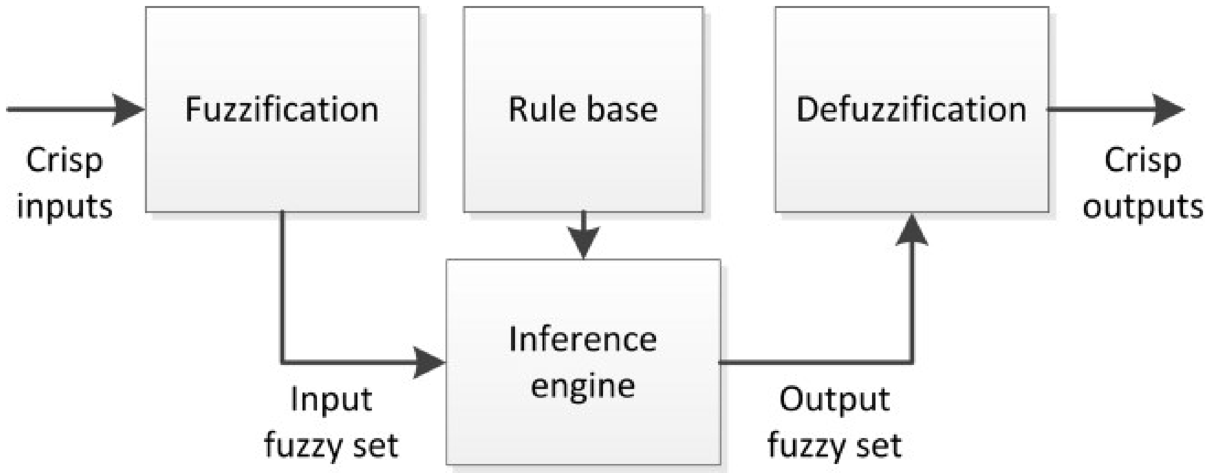

Figure 3. Block diagram of a fuzzy logic controller (FLC) architecture.

3.1.2. Fuzzy PI (FPI) Controller Design

The performance of the PI controllers deteriorates and loses tuning accuracy when the system experiences sudden parameter uncertainties or disturbances. This can result in reduced effectiveness and compromised control in response to unexpected variations or external influences. Therefore, the FPI controller is needed to modify the PI controller parameters in accordance with the error function. Fuzzy IF-THEN rules developed for FPI and FSMC controllers based on expert knowledge are shown in Table 2.

Table 2. FPI and FSMC IF–THEN rules.

Input Membership Functions		**Output Membership Functions**		**IF–Then Rules**
S. No.	Linguistic Terms	Linguistic Terms	If Input $\lvert e(t) \rvert$	Then (k_p, k_i)
1	Zero	Zero	Zero	Zero
2	Small	Small	Small	Small
3	Large	Large	Large	Large

The mathematical representation of the PI controller is,

$$u(t) = k_p e(t) + k_i \int e(t)dt \tag{10}$$

where $e(t) = V_{pv} - V_{ref}$ and k_p and k_i are proportional and integral gains of the PI controller, respectively. The above Equation (10) states that the PI's parameters are fixed and need to be adjusted to compensate for parameter uncertainties, load fluctuations, and electrical fault perturbations. Then, the updated equation of the controller is,

$$\lambda e(t) = A_1 L_1 e(t) + A_2 L_2 \int e(t)dt \tag{11}$$

where A_1 and A_2 are the fuzzy logic controller's outputs and L_1 and L_2 are learning rate constants for k_p and k_i, respectively. Figure 4 depicts the FPI block diagram.

3.2. Fuzzy Sliding Mode Controller (FSMC)

The structure of the FSMC consists of an FPI and an SMC, resulting in an enhanced ability to handle nonlinearity. FSMC combines the features of both controllers. Firstly, to reduce chattering in response, FPI is active in a steady state. By using fuzzy IF–THEN rules, the parameters of FPI, k_p, and k_i are updated. Throughout the transient state of the fuzzy system, the SMC is active. It enhances system stability and provides a fast dynamic response. Figure 5 represents the FSMC block diagram.

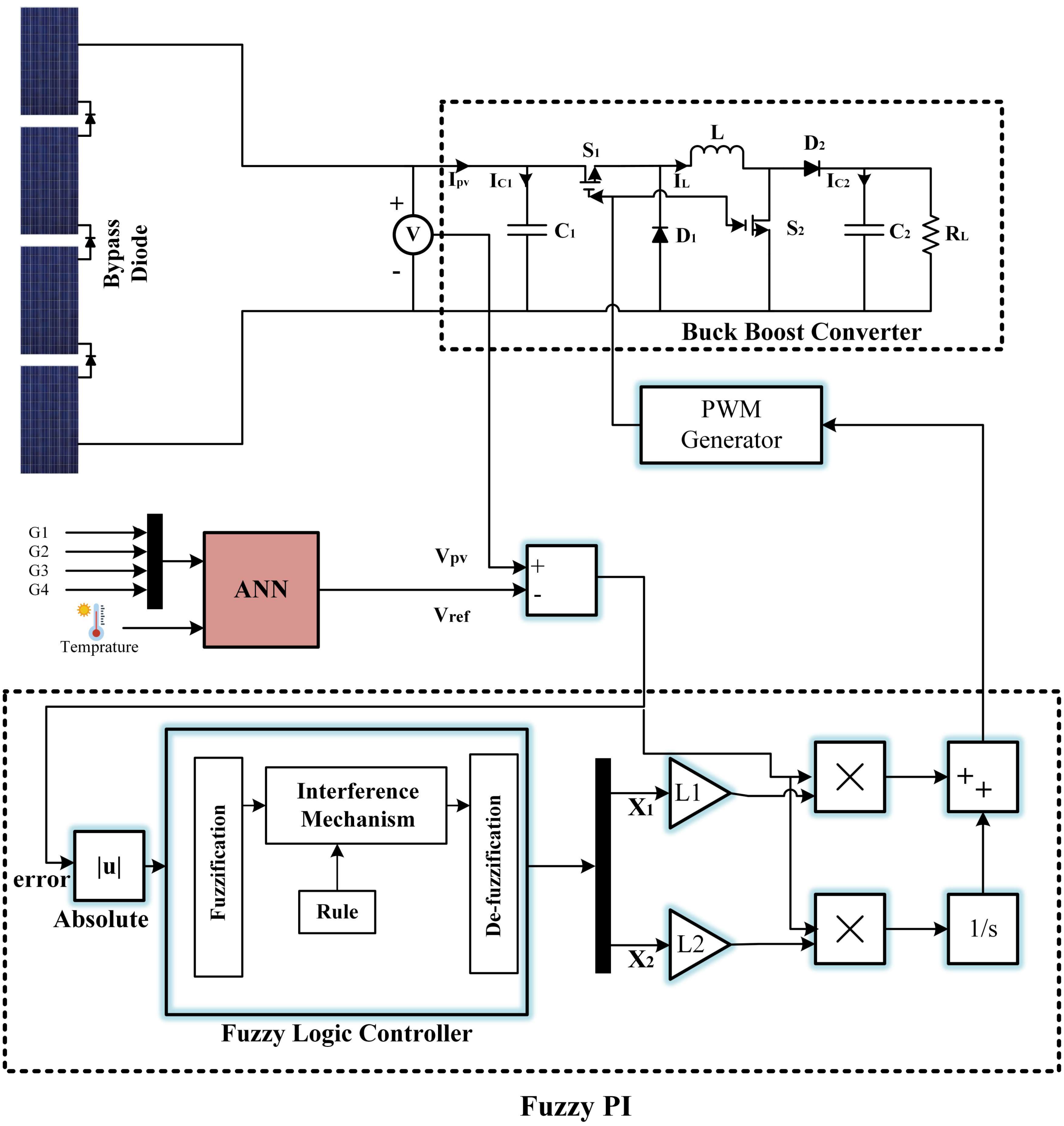

Figure 4. Block diagram of a fuzzy PI controller.

The initial stage entails the computation of the sliding surface, a crucial component in the control methodology. Subsequently, a control law is devised to enable the controller to swiftly track the reference signal. By employing this control law, the controller can promptly and accurately respond to any deviations from the desired reference, ensuring precise and efficient tracking performance. The sliding surface can be written as,

$$s = e(t) + \lambda e(t) \tag{12}$$

where,

$$e = V_{pv} - V_{ref} \tag{13}$$

Furthermore, $\lambda\, e(t)$ is,

$$\lambda e(t) = A_1 L_1 e(t) + A_2 L_2 \int e(t)dt \tag{14}$$

$\lambda e(t)$ is updated by using the FPI controller.

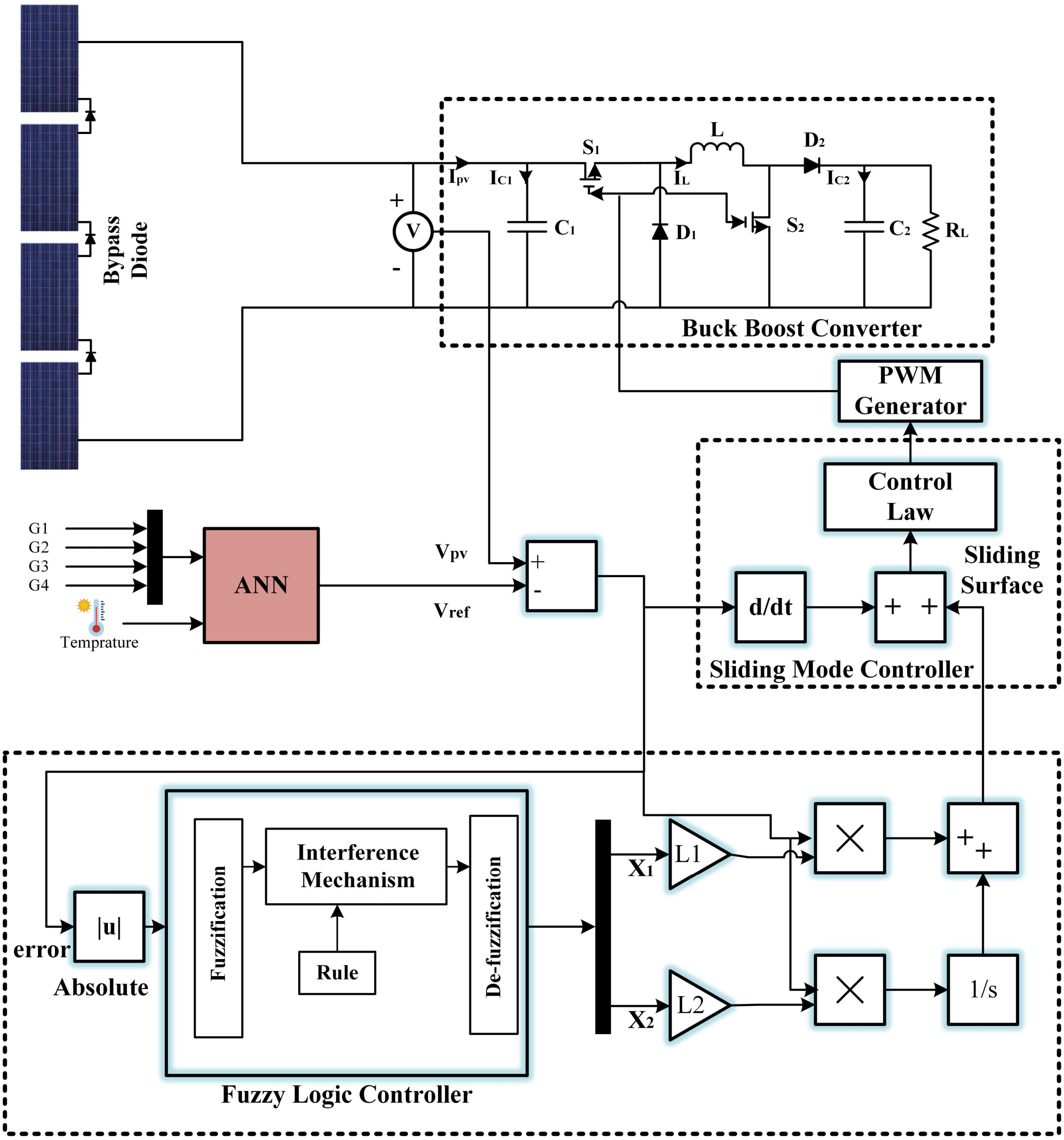

Figure 5. Block diagram of a fuzzy sliding mode controller.

By assuming $y = \lambda e(t)$, we obtain,

$$s = e(t) + y \tag{15}$$

We take the derivative of the sliding surface,

$$\dot{s} = \dot{e}(t) + \dot{y} \tag{16}$$

Put $\dot{s} = 0$ to calculate the control law,

$$\dot{e}(t) + \dot{y} = 0 \tag{17}$$

By adding the value of $e(t)$ in the equation,

$$\dot{V_{pv}} - \dot{V_{ref}} + \dot{y} = 0 \tag{18}$$

From Equation (9),

$$\dot{V_{pv}} = \dot{x_1} = \frac{I_{pv}}{C_i} - \frac{x_2}{C_i}u \tag{19}$$

By putting the value of $\dot{V_{pv}}$ in Equation (9),

$$\frac{I_{pv}}{C_i} - \frac{x_2}{C_i}u - \dot{V_{ref}} + \dot{y} = 0 \tag{20}$$

Simplifying the equation, we obtain the control law,

$$u_{eq} = u = \frac{C_i}{x_2}\left(\frac{I_{pv}}{C_i} - \dot{V_{ref}} + \dot{y}\right) \tag{21}$$

The discontinuous control law is defined as,

$$u_{dis} = -K_1(s) - K_2 sign(s) \tag{22}$$

The final equation of the control law is,

$$u = \frac{C_i}{x_2}\left(\frac{I_{pv}}{C_i} - \dot{V_{ref}} + \dot{y}\right) - K_1(s) - K_2 sign(s) \tag{23}$$

4. Results and Discussion

4.1. Voltage Tracking and Power Extracted by the Proposed Technique

In the proposed approach, as seen in Figure 6a, FPI and FSMC exactly follow the reference voltage and provide quick convergence. When the shading pattern moves from SP1 to SP2 with a temperature of 298.5 K, as mentioned in Table 1, the proposed algorithm follows the reference voltages, but P&O left the path and also has oscillations. The proposed technique has minimum chattering around MPP. Figure 6b depicts the output power of a PV array under SP1 and SP2 shading patterns. At 0.7 s, when the shading pattern moves from SP1 to SP2, the proposed approaches extract power without deviation and adhere to the reference; however, P&O cannot handle the rapid change, and it is not suitable for fast-changing environmental conditions. Likewise, in Figure 6a,b, it can also be observed that the transient response to the shading pattern lags in SMC compared to FPI and FSMC.

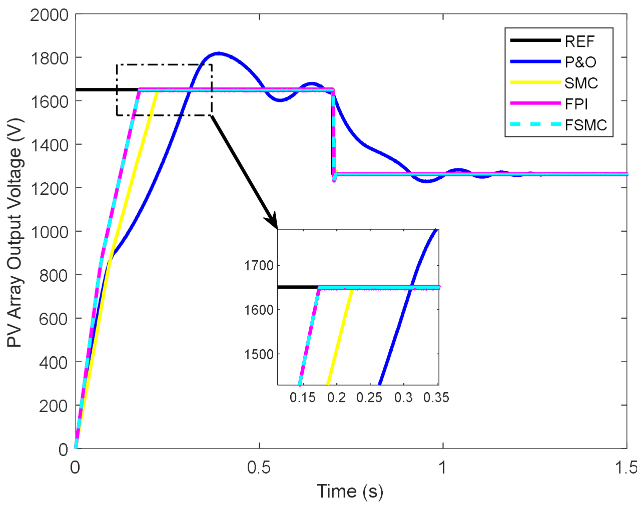

(**a**)

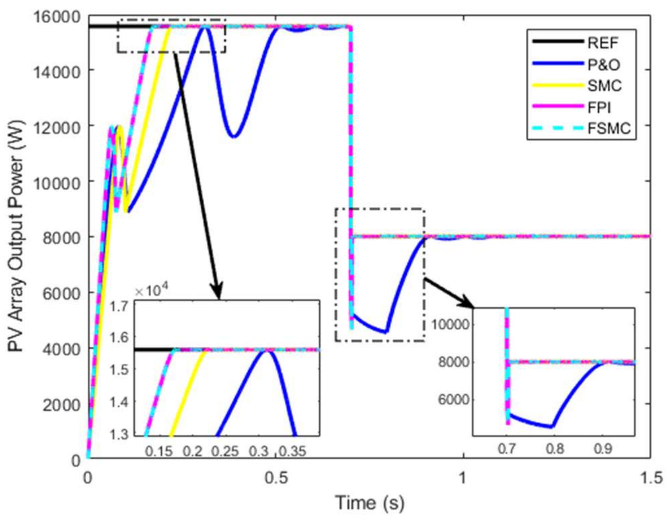

(**b**)

Figure 6. (**a**) Comparison of tracking voltage with different Techniques; (**b**) PV array output power at different shading patterns.

4.2. The Proposed Technique for Voltage Tracking and Power Extraction under Fault

However, partial shadowing presents the most challenging and insecure situation. In addition, the resilience of the established control systems is tested by introducing a sensor fault into the main channel x_1. of the PV system. The magnitude of the fault is as follows,

$$x_{1f} = x_1 + 60e^{\left(\left(\frac{2\pi}{4}\right)t\right)+45cos(2\pi t)}, \tag{24}$$

During the fault time (from 0.25 to 0.30 s), the system is studied. Under faulty situations, the proposed controllers outperform other approaches significantly in terms of voltage tracking and PV output power variation. The proposed controllers quickly retrack the reference and reach a steady state, as demonstrated in Figure 7a,b.

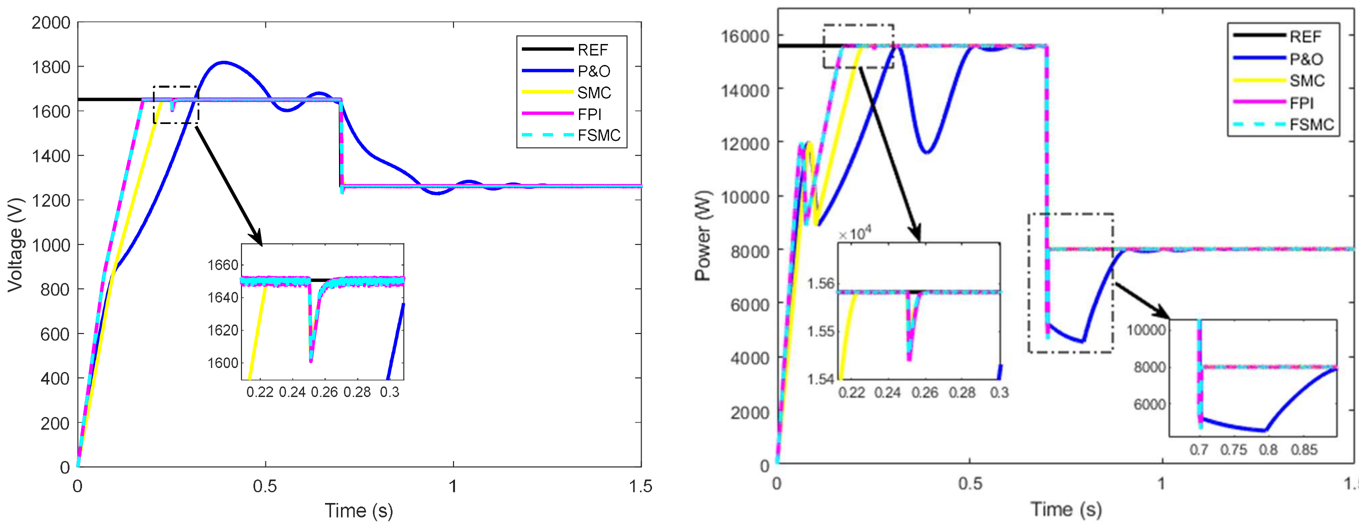

(**a**) (**b**)

Figure 7. (**a**) Voltage comparison under fault condition; (**b**) power comparison under fault condition.

4.3. Performance Indices Calculation

The performance of the system is evaluated by computing various errors, including integral absolute error, integral square error, integral time absolute error, and integral time square error. These errors are referred to as performance indices of the controllers. The performance of the proposed controllers is assessed in terms of these performance indices, which ensures minimal error in various scenarios.

Initially, we calculated and compared the performance indices of the PV system under partial shading conditions. The results demonstrate that the proposed control techniques exhibit the least error and superior performance compared to conventional controllers. Figure 8 provides a comprehensive comparison of the proposed techniques (FPI and FSMC) with the P&O and SMC methods in terms of performance indices.

In Figure 8a, the integral square error (ISE) is compared, and it shows that the proposed techniques (FPI and FSMC) have the lowest ISE values, indicating better performance compared to P&O and SMC. Meanwhile, Figure 8b focuses on the integral absolute error (IAE), and it demonstrates that FPI and FSMC outperform the other techniques, as they exhibit better results with lower IAE values. Additionally, Figure 8c compares the integral time square error (ITSE). Here, it is shown that FPI and FSMC have lower error values, suggesting improved performance when compared to the other methods.

Lastly, Figure 8d evaluates the integral time absolute error (ITAE) under partial shading conditions. The results indicate that the proposed techniques (FPI and FSMC) achieve less error and demonstrate better performance compared to P&O and SMC.

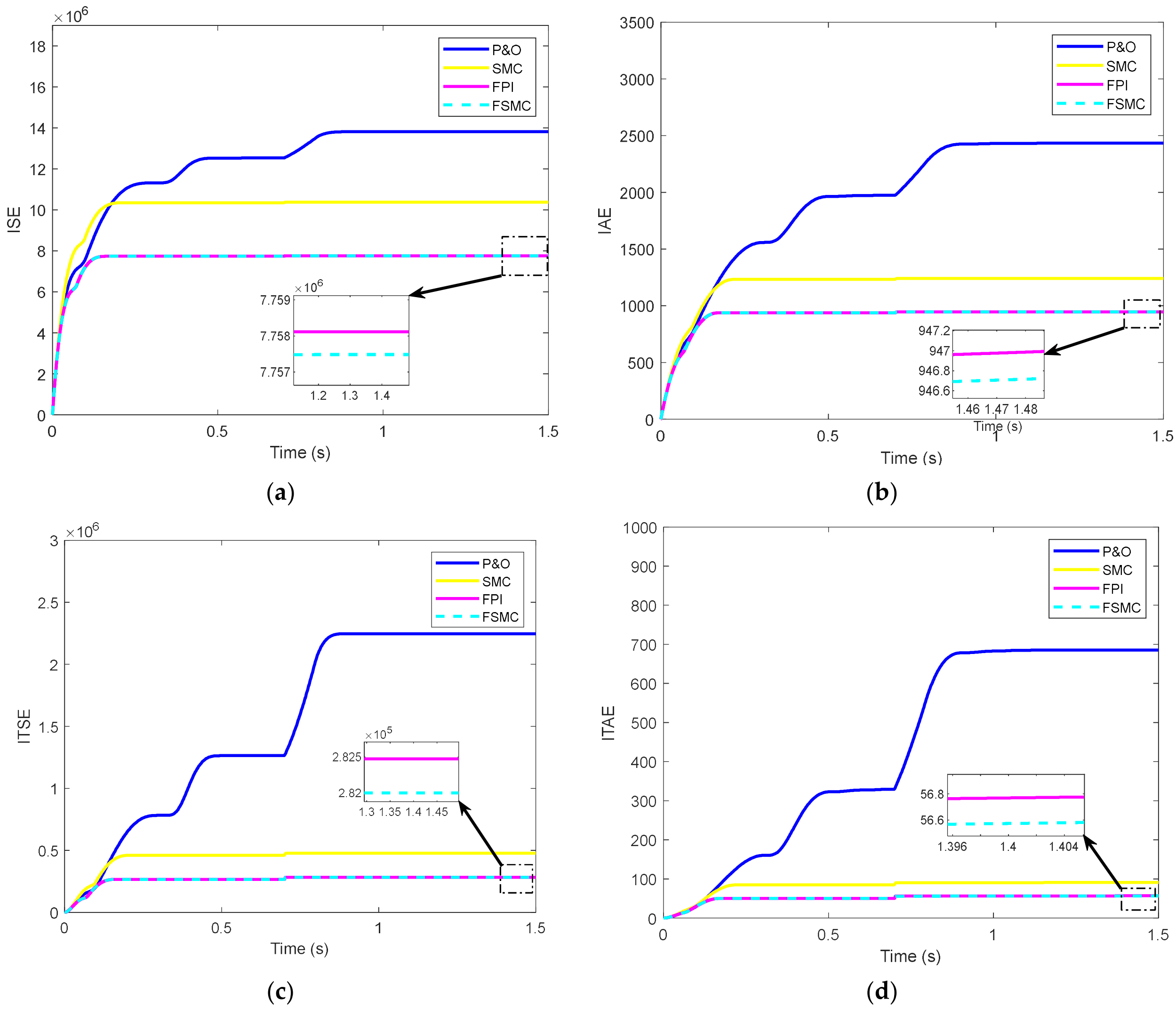

Figure 8. (**a**) Integral square error; (**b**) integral absolute error; (**c**) integral time square error; (**d**) integral time absolute error.

5. Conclusions

Under partially shading situations, the FPI and FSMC are designed and implemented in this paper. The neural network has been trained to produce the reference voltage for tracking of the GMPP by using the proposed controllers. The performance of the proposed controllers is compared with conventional controllers (P&O and standard sliding mode) in terms of voltage tracking, error, and power. Under partial shading conditions, the proposed techniques precisely track the reference voltage and maximum power, respectively, and provide relatively fast convergence. The resilience of the proposed controllers is also evaluated by inserting faults into the sensors of the PV system, even though partial shading is also an unclear, worst case scenario. Under faulty conditions, the proposed controllers performed much better in reference voltage tracking and PV output power extraction than the conventional approaches, even in the presence of fault. The performance of the system is also evaluated by calculating and comparing the various errors, which are known as performance indices. Integral absolute error, integral square error, integral time absolute error, and integral time square error are the four types of errors. In terms of performance indices, the proposed controllers also ensure the least error in all possible circumstances. Minor chattering is still a problem, although there are several ways to deal with the chattering effect. Further, the proposed techniques may be used in grid-connected systems as well as wind energy systems in hybrid configurations.

Author Contributions: Conceptualization, M.B.Q. and M.A.R.; methodology, M.A.R.; software, M.A.R.; validation, M.B.Q., M.A.R. and M.M.K.; formal analysis, M.A.R.; investigation, M.A.R.; resources, P.P. and S.A.A.Q.; data curation, M.B.Q. and M.A.R.; writing—original draft preparation, M.A.R. and M.B.Q.; writing—review and editing, M.A.R., M.M.K., P.P. and S.A.A.Q.; visualization, M.B.Q. and M.A.R.; supervision, M.B.Q.; project administration, M.B.Q. and M.M.K.; funding acquisition, P.P. and S.A.A.Q. All authors have read and agreed to the published version of the manuscript.

Funding: This research is funded by research supporting project number (RSPD2023R585, King Saud University, Riyadh, Saudi Arabia).

Data Availability Statement: Not applicable.

Conflicts of Interest: The authors declare no conflict of interest.

Appendix A

The PV cell electrical circuit regarding one diode model is presented in Figure A1.

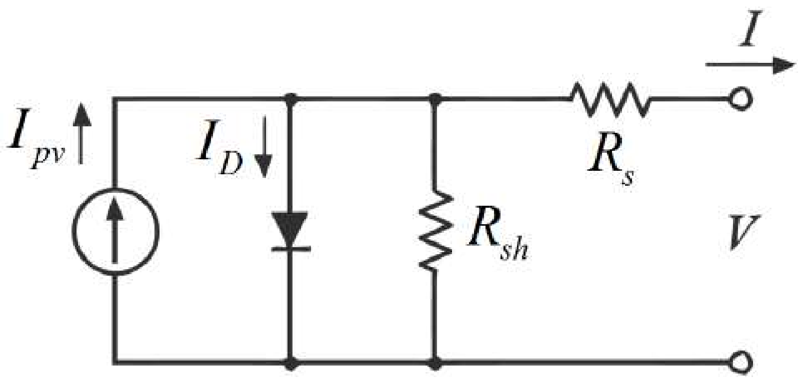

Figure A1. Solar cell equivalent circuit.

The current equation is written as,

$$I = I_{Pv}N_p - I_0N_p\left[exp\left(\frac{v + R_s\left(\frac{N_s}{N_p}\right)\mathrm{I}}{V_t a N_s}\right) - 1\right] - \frac{\nu + R_s\left(\frac{N_s}{N_p}\right)I}{R_p N_p} \quad \text{(A1)}$$

where

I_{Pv}: PV array current
N_s: series connected cell
N_p: parallel connected cell
I_0: saturation current of diode
R_s : resistance linked in series
R_p: resistance connected in parallel
V_t: thermal voltage
a: ideal factor (PV technology dependent)
The PV system's thermal voltage is,

$$V_t = \frac{N_s kT}{q} \quad \text{(A2)}$$

where

N_s: cell integrated in series
k: the Boltzmann's constant = 1.38×10^{-23} J/K
T: temperature of the P–N junction
q: charge of electron = 1.6×10^{-19} C
The photovoltaic current is,

$$I_{Pv} = \left(I_{pv,n} + K_I \Delta T\right)\frac{G}{G_n} \quad \text{(A3)}$$

where

$I_{pv,n}$: PV current in nominal conditions (1000 w/m^2)

K_I: short circuit current temperature coefficient

G: irradiance at that PV surface

G_n: radiance is the specified circumstance

$$\Delta T = T - T_n \tag{A4}$$

where,

T: actual temperature

T_n: nominal temperature

The diode's saturation current is,

$$I_0 = I_{0,n}\left(\frac{T_n}{T}\right)^3 exp\left[\frac{qE_g}{aK}\left(\frac{1}{T_n} - \frac{1}{T}\right)\right] \tag{A5}$$

where

$I_{0,n}$: under normal conditions, reverse saturation current

E_g: semiconductor energy bandgap (Eg ≈ 1.12 eV)

The nominal saturation current is,

$$I_{0,n} = \frac{I_{sc,n}}{exp\left(\frac{V_{oc,n}}{aV_{t,n}}\right) - 1} \tag{A6}$$

where

$I_{sc,n}$: saturation current under nominal conditions

$V_{oc,n}$: under nominal conditions, open circuit voltage

$V_{t,n}$: under the "nominal temperature situation", thermal voltage

Table A1. Photovoltaic (PV) panel parameters.

Sr. No.	Parameters	Values
1	Maximum Power	200 W
2	Cells in Each Module	54
3	Open Circuit Voltage	32.9 V
4	Optimum Voltage	26.3 V
5	Short Circuit Voltage	8.21 A
6	Optimum Current	7.61 A
7	Temperature Coefficient I_{sc}	0.00318 A/°C
8	Temperature Coefficient V_{oc}	−0.123 A/°C
9	Parallel Resistance	601.3368 Ω
10	Series Resistance	0.23 Ω

Table A2. Buck–boost converter's parameters.

Sr. No.	Parameters	Values
1	C1	13,000 uF
2	C2	68 uF
3	L	17 mH
4	RL	50 Ohms

Table A3. FPI and FSMC parameters.

Controller	Parameters	Values
FPI	A_1	10
	A_2	0.1
FSMC	A_1	100
	A_2	1
	$K1$	300
	$K2$	250

References

1. Ostadrahimi, A.; Mahmoud, Y. Novel Spline-MPPT Technique for Photovoltaic Systems under Uniform Irradiance and Partial Shading Conditions. *IEEE Trans. Sustain. Energy* **2021**, *12*, 524–532. [CrossRef]
2. Kurtz, S.; Repins, I.; Metzger, W.K.; Verlinden, P.J.; Huang, S.; Bowden, S.; Tappan, I.; Emery, K.; Kazmerski, L.L.; Levi, D. Historical Analysis of Champion Photovoltaic Module Efficiencies. *IEEE J. Photovolt.* **2018**, *8*, 363–372. [CrossRef]
3. Marks-Bielska, R.; Bielski, S.; Pik, K.; Kurowska, K. The Importance of Renewable Energy Sources in Poland's Energy Mix. *Energies* **2020**, *13*, 4624. [CrossRef]
4. Ahmed, M.A.; Eltamaly, A.M.; Alotaibi, M.A.; Alolah, A.I.; Kim, Y.C. Wireless Network Architecture for Cyber Physical Wind Energy System. *IEEE Access* **2020**, *8*, 40180–40197. [CrossRef]
5. Yang, X.; Song, Y.; Wang, G.; Wang, W.; Yang, X.; Song, Y.; Wang, G.; Wang, W. A Comprehensive Review on the Development of Sustainable Energy Strategy and Implementation in China. *IEEE Trans. Sustain. Energy* **2010**, *1*, 57–65. [CrossRef]
6. Nurunnabi, M.; Roy, N.K.; Hossain, E.; Pota, H.R. Size Optimization and Sensitivity Analysis of Hybrid Wind/PV Micro-Grids-A Case Study for Bangladesh. *IEEE Access* **2019**, *7*, 150120–150140. [CrossRef]
7. Zeb, K.; Khan, I.; Uddin, W.; Khan, M.A.; Sathishkumar, P.; Busarello, T.D.C.; Ahmad, I.; Kim, H.J. A Review on Recent Advances and Future Trends of Transformerless Inverter Structures for Single-Phase Grid-Connected Photovoltaic Systems. *Energies* **2018**, *11*, 1968. [CrossRef]
8. Tatabhatla, V.M.R.; Agarwal, A.; Kanumuri, T. Performance Improvement by Mitigating the Effects of Moving Cloud Conditions. *IEEE Trans. Power Electron.* **2021**, *36*, 4214–4223. [CrossRef]
9. Chen, K.; Tian, S.; Cheng, Y.; Member, S.; Bai, L. An-Improved-MPPT-Controller-for-Photovoltaic.Pdf. 2014, pp. 1–8. Available online: https://www.semanticscholar.org/paper/An-Improved-MPPT-Controller-for-Photovoltaic-System-Chen-Tian/fba0443b4b250a68675efb6132b34ae1f2963aee (accessed on 8 June 2023).
10. Gosumbonggot, J.; Fujita, G. Partial Shading Detection and Global Maximum Power Point Tracking Algorithm for Photovoltaic with the Variation of Irradiation and Temperature. *Energies* **2019**, *12*, 202. [CrossRef]
11. Roy Chowdhury, S.; Saha, H. Maximum Power Point Tracking of Partially Shaded Solar Photovoltaic Arrays. *Sol. Energy Mater. Sol. Cells* **2010**, *94*, 1441–1447. [CrossRef]
12. Safari, A.; Mekhilef, S. Implementation of Incremental Conductance Method with Direct Control. In *TENCON 2011–2011 IEEE Region 10 Conference*; IEEE: Piscataway, NJ, USA, 2011; pp. 944–948. [CrossRef]
13. Chao, K.H.; Rizal, M.N. A Hybrid Mppt Controller Based on the Genetic Algorithm and Ant Colony Optimization for Photovoltaic Systems under Partially Shaded Conditions. *Energies* **2021**, *14*, 2902. [CrossRef]
14. Obukhov, S.; Ibrahim, A.; Zaki Diab, A.A.; Al-Sumaiti, A.S.; Aboelsaud, R. Optimal Performance of Dynamic Particle Swarm Optimization Based Maximum Power Trackers for Stand-Alone PV System under Partial Shading Conditions. *IEEE Access* **2020**, *8*, 20770–20785. [CrossRef]
15. Guenounou, O.; Dahhou, B.; Chabour, F. Adaptive Fuzzy Controller Based MPPT for Photovoltaic Systems. *Energy Convers. Manag.* **2014**, *78*, 843–850. [CrossRef]
16. Naghmash; Armghan, H.; Ahmad, I.; Armghan, A.; Khan, S.; Arsalan, M. Backstepping Based Non-Linear Control for Maximum Power Point Tracking in Photovoltaic System. *Sol. Energy* **2018**, *159*, 134–141. [CrossRef]
17. Syafaruddin; Karatepe, E.; Hiyama, T. Artificial Neural Network-Polar Coordinated Fuzzy Controller Based Maximum Power Point Tracking Control under Partially Shaded Conditions. *IET Renew. Power Gener.* **2009**, *3*, 239–253. [CrossRef]
18. Kumar, N.; Hussain, I.; Singh, B.; Panigrahi, B.K. Rapid MPPT for Uniformly and Partial Shaded PV System by Using JayaDE Algorithm in Highly Fluctuating Atmospheric Conditions. *IEEE Trans. Ind. Inform.* **2017**, *13*, 2406–2416. [CrossRef]
19. Kihal, A.; Krim, F.; Laib, A.; Talbi, B.; Afghoul, H. An Improved MPPT Scheme Employing Adaptive Integral Derivative Sliding Mode Control for Photovoltaic Systems under Fast Irradiation Changes. *ISA Trans.* **2019**, *87*, 297–306. [CrossRef]
20. Kihal, A.; Krim, F.; Laib, A. MPPT Voltage oriented Loop Based on Integral Sliding Mode Control to the Boost Converter. In Proceedings of the International Conference on Systems and Control (ICSC), Batna, Algeria, 7–9 May 2017; IEEE: Piscataway, NJ, USA, 2017; ISBN 9781509039609.
21. Farhat, M.; Barambones, O.; Sbita, L. A New Maximum Power Point Method Based on a Sliding Mode Approach for Solar Energy Harvesting. *Appl. Energy* **2017**, *185*, 1185–1198. [CrossRef]

22. Sajadian, S.; Ahmadi, R. Model Predictive-Based Maximum Power Point Tracking for Grid-Tied Photovoltaic Applications Using a Z-Source Inverter. *IEEE Trans. Power Electron.* **2016**, *31*, 7611–7620. [CrossRef]
23. Sajadian, S.; Ahmadi, R. Distributed Maximum Power Point Tracking Using Model Predictive Control for Solar Photovoltaic Application. In Proceedings of the Thirty Second Annual IEEE Applied Power Electronics Conference and Exposition, Tampa, FL, USA, 26–30 March 2017; IEEE: Piscataway, NJ, USA, 2017; ISBN 9781509053667.
24. Aguilera, R.P.; Quevedo, D.E. On Stability and Performance of Finite Control Set MPC for Power Converters. In Proceedings of the Workshop on Predictive Control of Electrical Drives and Power Electronics, Munich, Germany, 14–15 October 2011; IEEE: Piscataway, NJ, USA, 2011; ISBN 9781457719141.
25. Ahmad, W.; Qureshi, M.B.; Khan, M.M.; Fayyaz, M.A.; Nawaz, R. Optimizing Large-Scale PV Systems with Machine Learning: A Neuro-Fuzzy MPPT Control for PSCs with Uncertainties. *Electronics* **2023**, *12*, 1720. [CrossRef]